Optimization of Multi-Stage Neuroblastoma Therapy Based on Differential Transformations

***Andrii Gusynin*[1], *Alexander Haupt*[2]**

[1] *Sanifons UG, Germany;* [2] *Military Forces of Ukraine*

Abstract. A numerical-analytical method for optimizing multi-stage high-risk neuroblastoma therapy is proposed, based on the differential transform method and a terminal control framework. The mathematical model of the "tumor-neuropil-immunity-pharmacokinetics" system is formulated in spectral form, enabling optimal control synthesis without numerical integration of the system of differential equations. The proposed approach yields a compact recurrent representation of the dynamics, an analytical form of the optimal control law, and a closed-loop control algorithm robust to parameter perturbations and individual patient responses. It is shown that the method provides significant computational acceleration compared to gradient-based optimization, making it suitable for near-real-time clinical decision support systems.

Keywords: *neuroblastoma; optimal control; multi-stage therapy; differential transform method; pharmacokinetics; immune response; spectral models*

1. Introduction

High-risk neuroblastoma remains one of the most aggressive solid tumors of childhood, and treatment efficacy is largely determined by the ability to maintain a balance between anti-tumor activity and preservation of a functional immune response [1,2]. Standard chemotherapy protocols are based on fixed dosing regimens that do not account for the individual dynamics of the "tumor-immunity-pharmacokinetics" system and its pronounced nonlinearity and non-stationarity [3,4]. This limits the possibility of personalized therapy and increases the risk of toxic complications, which is critically important in pediatric oncology [2].

Contemporary studies demonstrate that the tumor microenvironment, in particular the level of tumor-infiltrating lymphocytes (TIL), immune activity, and transcriptomic subtypes, constitute key prognostic factors for neuroblastoma [5-8]. This has stimulated the development of mathematical models capable of describing the interaction of tumor cells, immune response, and cytostatic pharmacokinetics. Early approaches based on competitive Lotka-Volterra-type models described tumor-immune cell interactions but did not account for the complexity of the tumor microenvironment. Further development was achieved by immunological models, including the Wilkie-Hahnfeldt system and immune checkpoint models, which formalize mechanisms of immune surveillance, cytotoxic activity, and immune evasion [9-11]. In parallel, pharmacokinetic and pharmacodynamic (PK/PD) models were developed that describe absorption, distribution, and elimination of cytostatics and allow evaluation of toxicity and therapeutic effect in pediatric patients [12-15]. Hybrid models combine these approaches, integrating immune response, pharmacological effects, and tumor microenvironment [9-11].

Despite significant progress, most existing models focus on dynamic analysis rather than control synthesis. Dosing optimization is typically performed by numerical methods, which are computationally expensive, sensitive to parametric uncertainty, and do not yield an analytical control form suitable for clinical application. Optimal control methods, including the Pontryagin maximum principle, dynamic programming, and Hamilton-Jacobi-Bellman equations, are actively applied to anti-tumor therapy optimization [16-20]. However, their practical use in biomedical models is substantially limited: optimality conditions take the form of implicit high-dimensional nonlinear systems, numerical algorithms are slow and sensitive to parametric uncertainty, and the resulting strategies rarely have a closed analytical form suitable for real-time application [16,17]. Furthermore, in a number of works the immune response is erroneously treated as a controlled variable, whereas it is an internal physiological process that should be regarded as a constraint rather than an optimization target [9-11]. Most existing approaches also fail to account for the time-varying nature of therapy parameters, although clinically the "tumor–immunity–pharmacokinetics" system dynamics are substantially non-stationary.

The differential transform method (DTM) has been extensively developed and applied in nonlinear system modeling and control [21-23], and its extensions have recently been explored in biomedical and physiological modeling **[**24-27**]**. These studies have demonstrated that spectral representations provide stable and computationally efficient approximations for nonlinear biological dynamics, motivating their use in optimal therapy design. However, in its classical form DTM contains no mechanisms for control synthesis and does not incorporate terminal constraints, which limits its application to optimal dosing problems.

The approach proposed in this work represents an example of interdisciplinary technology transfer: methods developed for nonlinear systems with terminal constraints have been adapted to problems of mathematical oncology. In nonlinear terminal control problems, program parameters are determined through spectral coefficients of differential transforms;

the same principle is transferred to multi-phase therapy, where each stage has its own target states and constraints. Such a transfer makes it possible to obtain analytical formulas for therapeutic intervention parameters and provides the high computational efficiency required for clinical applications [28-32].

In this work, a numerical-analytical method for synthesizing multi-stage terminal control for the "tumor-immunity-pharmacokinetics" system is proposed, combining the spectral properties of DTM with a terminal control framework. Optimization is performed under the criterion of minimizing tumor mass, while drug concentration and immune response are treated as pharmacological and physiological constraints, respectively.

2. Mathematical Model and Parametrization

As the controlled plant we consider the mathematical model of neuroblastoma of "tumor–neuropil–immunity" type with drug pharmacokinetics:

$$\dot{c} = -k_e c + k_a u(t), \tag{1}$$

$$\dot{x} = \alpha x\left(1 - \frac{x}{K}\right) - \beta x p - \kappa x z - \gamma c x, \tag{2}$$

$$\dot{p} = \mu x - \delta p, \tag{3}$$

$$\dot{z} = \sigma x - \lambda z - \varphi c z, \tag{4}$$

where $x(t)$ is the density of tumor cells (neuroblasts), $p(t)$ is the neuropil density, $z(t)$ is the intensity of the immune response, $c(t)$ is the drug concentration, and $u(t)$ is the therapeutic input (chemotherapy intensity). The parameters $\alpha, \beta, \kappa, \mu, \delta, \lambda, K$ are determined by morphometric and immunological characteristics of the tumor [33-36]. The control $u(t)$ acts as a proliferation inhibitor, reducing the mitotic activity of tumor cells. Equation (1) corresponds to a single-compartment pharmacokinetic model with linear elimination [12].

To ensure clinical relevance, the parameters of model (1)-(4) are not arbitrary but are determined from the morphological and immunological characteristics of the tumor according to the Shimada classification [37]. As shown in [34], each system coefficient is a function of clinical markers: the nuclear-to-cytoplasmic ratio (RNC), mitotic–karyorrhectic index (MKI), neuropil density (η), and TIL level. In particular:

- α (proliferation rate) and K (carrying capacity) are modulated by morphometric indices of atypia and stromal maturity [33-36,38,39].
- Immune response parameters (κ, σ) depend directly on the TIL index [5,8].
- Depletion and toxicity parameters ($\lambda, \delta, \gamma, \varphi$) are determined by the integral systemic stress index (S) [12-15].

This approach allows the system (1)-(4) to be interpreted as a parametrized digital twin of the patient, since all model coefficients are directly determined by clinical markers. For numerical computations, all clinical input indicators are normalized to the interval $[0,1]$, which ensures computational stability of the spectral models [21-23].

3. Multi-Stage Terminal Control Problem Formulation

The entire multi-stage treatment process on the interval $[t_0, T]$ is partitioned into r prescribed time intervals (therapy stages). We assume that within each interval the state vector variables are continuous, while discrete changes in parameters or intervention intensity occur at interval boundaries:

$$T_i = t_i - t_{i-1}, i = \overline{1,r}, \sum_{i=1}^{r} T_i = T,$$

where T is the total duration of the controlled therapy process, which depending on the clinical problem statement may be fixed according to a medical protocol or left free for optimization of the time resource for reaching the terminal goal.

On each time interval, the state dynamics of the controlled plant are described by the vector differential equation:

$$\frac{dx_i}{dt} = f_i(t, x_i, u_i, \xi_i), x_i(t_{i-1}) = x_i^0, i = \overline{1,r}. \tag{5}$$

where x_i is the n-dimensional state vector (tumor density, immunity level, etc.); u_i is the m-dimensional control vector (drug infusion rate); ξ_i is the ℓ-dimensional disturbance vector (individual response, systemic stress); f_i is a vector-function of generalized forces that is continuous and continuously differentiable with respect to the variable t, x_i, u_i, ξ_i on each time interval; and $t \in (t_i - t_{i-1})$ is the current (local) time within the i-th interval.

The terminal control problem consists of transferring the system from the prescribed initial state $x_i(t_0) = x_{i_0}$ to the terminal state $x_r(T)$, specified at $t = T$ by the q-dimensional ($q \leq n$) equation:

$$S[x_r(T), T] = 0 \tag{6}$$

The effectiveness of the treatment process is evaluated by the quality functional:

$$I = G[x_r(T), T] + \sum_{i=1}^{r} \int_{t_0}^{T} \Phi_i(t, x_i, u_i, \xi_i) dt, \tag{7}$$

where the prescribed functions G and Φ_i have continuous partial derivatives with respect to x_i, u_i, ξ_i on each time interval and define the criteria for minimizing tumor mass subject to constraints on systemic toxicity. Constraints on state and

control vectors are incorporated directly into the structure of functional (7) via corresponding weighting coefficients or penalty functions.

According to the multi-stage control concept, the matching of boundary and initial conditions at therapy stage transitions (e.g., from induction to consolidation) is achieved through prescribed boundary conditions:

$$\varphi_i[x_i(T_i), x_{i+1}^0; u_i(T_i), u_{i+1}^0; T_i] = 0, i = \overline{1,r}. \quad (8)$$

The multi-stage terminal control problem (5)-(8) is solved sequentially. First, the optimal control $u_1(t)$ is determined on the first interval $t_0 \le t \le t_1$ with initial condition $x_1(t_0) = x_{1_0}$. The computed state vector at the end of the stage, $x_1(t_1)$, becomes the initial condition for the second stage on $[t_1, t_2]$. The resulting state trajectory $x(t)$ and control function $u(t)$ are continuous everywhere on $[t_0, T]$ and at junction points. Continuing this process yields a continuous piecewise-differentiable solution of (5) and the corresponding optimal control that, subject to the differential constraints (5), boundary conditions (6), and junction conditions (8), optimizes functional (7) in the absence of disturbances [40].

However, in real clinical conditions, the influence of unpredictable environmental factors and the individual physiological response $\xi_i(t)$ may lead to substantial terminal errors, either failure to achieve the required tumor destruction or exceeding the toxicity threshold, at the final time of the programmed control $u = u(t)$. To compensate for these disturbances, a feedback control law $u = u(x, t)$ is synthesized, which at each moment t uses information about the actual current state $x(t)$ of the biosystem. Feedback control ensures that the system can be driven from an arbitrary perturbed state to the prescribed terminal state even in the presence of disturbances. The synthesis of a feedback law $u = u(x, t)$ can be performed using dynamic programming [41], although this approach suffers from the curse of dimensionality, requiring extremely large memory resources even for systems of modest dimension.

4. Determination of Optimal Control

We apply the DTM to the multi-stage optimal control problem for a biosystem (the neuroblastoma therapy process). Differential transforms replace continuous-argument functions $x(t)$ with discrete-argument functions $X(k)$, $k = 0,1,2,..$, according to [21,22]:

$$\underline{x(t)} = X(k) = \frac{h^k}{k!}\left[\frac{d^k x(t)}{dt^k}\right]_{t=t_0}, \quad (9)$$

where $x(t)$ is a real analytic function of a real argument, $X(k)$ is a discrete function of the integer argument k, called the differential spectrum of $x(t)$ at $t = t_0$, and h is a scaling constant with the dimension of time. The underline symbol denotes the differential transform operator.

Models obtained via (9) are referred to as spectral models. We assume that all control functions within each time interval of problem (5)-(8) are analytic, while first-order discontinuities may occur at interval boundaries.

The synthesis of the optimal multi-stage feedback control is performed using the closure method applied to the optimal programmed control $u = u(t)$ for an arbitrary current state of the biosystem [22]. First, we consider the undisturbed (nominal) dynamics of the system. On each i-th stage of the control process, we choose the structure of the programmed control $u_i(\tau, A_i)$ from the class of analytic functions, where $A_i = (a_{i_1}, a_{i_2}, \dots a_{i_n})$ is the vector of free parameters and τ is the local time.

The differential transformation of $u_i(\tau, A_i)$ at $h = T_i$, $\tau = 0$ gives:

$$\underline{u_i}(\tau, A_i) = U_i(k, A_i) = \frac{T_i^k}{k!}\left[\frac{d^k u_i(t_{i-1}+\tau, A_i)}{dt^k}\right]_{\tau=0}. \quad (10)$$

The vector differential equation (5) is represented in the image domain as the spectral model:

$$X_i(k+1, A_i, X_i^0) = \frac{T_i}{k+1}\underline{f_i}[T_i, X_i(k, A_i, X_i^0), U_i(k, A_i)], \quad (11)$$
$$X_i(0) = X_i^0(A_{i-1}, A_{i-2}, \dots, A_1); X_1(0) = X_1^0 = x_0; i = \overline{1,r}.$$

Spectral model (11) is universal and can be applied to biosystem control problems of varying complexity. Since differential transformations (9) constitute an exact operational method for analytic functions, model (11) introduces no additional discretization error at the formula level and potentially yields a locally exact approximation to the solution of (5). This spectral model is a recurrent expression that makes it possible to construct the differential spectrum $X_i(k, A_i, X_i^0)$ of the state vector $x_i(t)$ from the differential spectrum (10) of the control function $u_i(\tau, A_i)$.

We use the property of differential transforms stating that the algebraic sum of all components (discretes) of the differential spectrum of any analytic function at $t = t_v$ is equal to the zero-order discrete of the differential spectrum at $t_{v+1} = t_v + h$, or equivalently, to the value of the original function at the same point.

$$\sum_{k=0}^{\infty} X_v(k) = X_{v+1}(0) = x(t_v + h). \quad (12)$$

From relation (12), taking $t_v = t_{i-1}$ and $h = T_i$, we obtain the state vector at the end of each i-th time interval of the control process:

$$x_i(T_i, A_i, x_i^0) = \sum_{k=0}^{\infty} X_i(k, A_i, X_i^0), i = \overline{1,r}. \quad (13)$$

The terminal condition (6) for the whole process, accounting for junction conditions (8) and expression (13), takes the form:

$$S[A_1, A_2, \ldots, A_r] = 0. \quad (14)$$

This boundary condition implicitly defines q components of the free-parameter vector A_i, $i = \overline{1,r}$ for each i-th interval, and qr components for the entire process, as functions of T_i and x_i^0.

Applying the differential transforms (9) to functional (7), considering the differential spectra (10) and (11), allows us to represent this functional as a function of the free-parameter vectors A_i:

$$I(A_1, A_2, \ldots, A_r) = G[A_1, A_2, \ldots, A_r] + \sum_{i=1}^{r} T_i \sum_{r=0}^{\infty} \frac{\Phi_i[T_i, X_i(k, A_i, X_i^0), U_i(k, A_i)]}{k+1}. \quad (15)$$

The necessary optimality conditions for functional (15) yield a system of equations for determining the remaining $n - q$ components of the free-parameter vectors for each i-th time interval, and $(n - q)r$ components for the entire control process [42]:

$$\frac{\partial I(A_1, A_2, \ldots, A_r)}{\partial a_{ij}} = 0; \quad i = \overline{1,r}; \quad j = \overline{q+1, n}. \quad (16)$$

A complete mathematical analysis of the convergence of the spectral model (11), the existence and uniqueness of the solution of systems (14) and (16), as well as error estimates for the optimal control, is presented in a separate publication [43]. In this article, we focus on the applied aspect of the method and its use in the problem of multi-stage neuroblastoma therapy.

The resulting nonlinear system of equations (14) and (16) implicitly defines all components of the free-parameter control vector $A = (A_1, A_2, \ldots, A_r)$ as functions of the arbitrary initial state vector $x_o = x_i(t_{i_0})$. Thus, an implicit nonlinear relationship is established between the optimal programmed control $u[t, A(T, x_0)]$, the initial state $x_0 = x_i(t_{i_0})$, the initial time t_{i_0}, and the total duration T of the multi-stage control process.

A formal analysis of the convergence of the spectral model (11) and the local solvability of systems (14) and (16) is given in [43]. In this article, we focus on the practical implementation of the method and its application to multi-stage neuroblastoma therapy.

In the presence of disturbances, the obtained programmed control cannot be applied over the entire time interval T, because it is valid only at the initial moment t_{i_0}. Therefore, the differential transforms (9) make it possible to obtain, in analytical form, the system of equations (14) and (16) for arbitrary values of the initial state $x_0 = x_i(t_{i_0})$, the initial time t_{i_0}, and the duration T of the multi-stage control process.

When disturbances act on the system, the object continuously deviates from the optimal programmed trajectory. In this case, the control $u[t, A(T, x)]$ is computed from systems (14) and (16) for the current values of time t and state $x(t)$. Thus, continuous-time solution of systems (14) and (16) forms the closed-loop multi-stage terminal control law $u = u(t, x)$. Solving systems (14) and (16) at each current moment t and state $x(t)$ of the disturbed dynamic object continuously yields the control $u = u(t, x)$, which links the current state $x(t)$ with the terminal conditions (6). In the closed-loop mode, only the current value of the control $u[t, A(T, x)]$ is applied, and at the next moment it is recomputed from systems (14) and (16). This provides flexible adaptation of the optimal trajectory to unknown disturbance factors $\xi(t)$.

If, in addition to the optimal programmed control vector, it is necessary to determine the components of the state vector $x_i(\tau, A_i)$, they can be obtained from the differential spectrum (11) in the form of truncated Taylor series, or via inverse differential transforms in the form of Legendre polynomials, Chebyshev polynomials, Fourier series, or combinations of various approximating functions [21,22]. The free parameters of the approximating functions are determined by matching the differential spectra of the state components with the differential spectra of the approximating functions.

It should be noted that the efficiency of the constructed model decreases as the dimension of the free-parameter control vector increases. Therefore, in practical problems it is advisable to restrict the dimension of this vector. It is also necessary to verify the existence of an extremum of functional (15) using sufficient optimality conditions.

5. Synthesis of the Optimal Control Algorithm

The proposed numerical-analytical method enables construction of an optimal anti-tumor drug administration algorithm. The core idea is the transfer of control principles developed for complex aerodynamic objects (specifically, airships during ascent) to the dynamics of biological systems.

In clinical oncology, neuroblastoma treatment is a strictly structured process consisting of sequential phases: induction, intensification, and consolidation. Each phase has unique target states and physiological constraints. Mathematically, this is justified by the time variation of system (1)-(4) parameters: proliferation coefficient α, immune cytolysis κ, and

systemic stress S are not static but evolve under treatment. Accordingly, partitioning the therapy trajectory into distinct stages is not only clinically necessary but also mathematically natural for handling system non-stationarity.
This stage-wise decomposition is also required because the system parameters (α, κ, S) are non-stationary and evolve during therapy, which mathematically necessitates treating each phase as a separate terminal control segment.

5.1. Structure of Controlled Therapy Stages

Analogously to aerostatic vehicle ascent stages, three key control segments are identified:

- Stage 1 ($i = 1$): Cytoreduction phase (Induction). Target: maximum rapid reduction of tumor mass $x(t)$. Dynamics: direct cytotoxic action γcx dominates; the system is under high load, analogous to initial aircraft acceleration.
- Stage 2 ($i = 2$): Immunomodulation phase. Target: state stabilization and activation of immune response $z(t)$ (TIL activity). Dynamics: parameters σ and κ increase; nonlinear competition arises between immune tumor suppression and toxic immune depletion, analogous to the transitional thrust-vector regime.
- Stage 3 ($i = 3$): Minimal residual disease control (Consolidation). Target: maintenance of a critically low tumor cell level with minimal systemic toxicity. Dynamics: the system becomes hypersensitive to small control changes, requiring high prediction accuracy analogous to precision maneuvering.

As the control, we adopt the drug infusion rate $u(t)$ given as a linear program in time:

$$u_i(t) = a_{0_i} + a_{1_i} t, \tag{17}$$

Where a_{0_i}, a_{1_i} are free parameters to be determined for each i-th therapy stage.
As the quality criterion for each stage we adopt:

$$I_i = x_i(T_i), \tag{18}$$

i.e., tumor mass is minimized at the end of the i-th stage subject to prescribed terminal constraints on immune response and drug concentration. The analogue of a "critical failure" in aerospace systems corresponds to irreversible immunosuppression or critical intoxication in neuroblastoma biodynamics, rendering further treatment impossible.
In general, the choice of the functional reflects the need to balance therapeutic efficacy against systemic toxicity, which is critical due to the narrow therapeutic window of cytotoxic drugs.
The terminal control problem on the i-th stage consists of transferring the system from initial conditions

$$x_i(0) = x_{i0}, z_i(0) = z_{i0}, c_i(0) = c_{i0} \tag{19}$$

to prescribed terminal states

$$x(T_i) = x_{T_i}, z(T_i) = z_{T_i}, c(T_i) = c_{T_i} \tag{20}$$

achieving the minimum of functional (18).

5.2. Spectral Model and Spectral Coefficients

To determine the terminal control algorithm, we compute the spectral coefficients (discrete components) of the differential spectra of the "drug–tumor–immunity" model (1)-(4). Applying the general spectral model (11) to system (1)-(4) yields the recurrence relations:

$$X(k+1) = \frac{h}{k+1} \underline{f_x}\left[X(k), Z(k), C(k), \underline{U}(k), \underline{t}\right], X(0) = x_0, \tag{21}$$

$$Z(k+1) = \frac{h}{k+1} \underline{f_z}\left[X(k), Z(k), C(k), \underline{t}\right], Z(0) = z_0, \tag{22}$$

$$C(k+1) = \frac{h}{k+1} \underline{f_c}\left[C(k), \underline{U}(k), \underline{t}\right], C(0) = c_0, \tag{23}$$

$$P(k+1) = \frac{h}{k+1} [\mu X(k) - \delta P(k)], P(0) = p_0, \tag{24}$$

In subsequent analysis, expression (24) is excluded from the spectral model owing to the quasi-stationary approximation $p = \frac{\mu}{\delta} x$, and the expansion is truncated at two to three spectral coefficients. As shown in prior studies [21], this truncation order is sufficient for acceptable accuracy in dynamic system control problems.
The spectral coefficients are expressed as functions of the initial state values, the free control parameters (a_0, a_1), and the duration T_i of the i-th therapy stage.
The zero-order coefficients coincide with the initial conditions (19):

$$X(0) = x_{i_0}, Z(0) = z_{i_0}, C(0) = c_{i_0} \tag{25}$$

The programmed control (17) in spectral form has coefficients:

$$U(0) = a_0, U(1) = T_i a_1, U(k) = 0, k \geq 2 \tag{26}$$

Restricting to two to three spectral coefficients, the first-order coefficients are:

$$X(1) = T_i F_{x_i}, \tag{27}$$

$$Z(1) = T_i\left[\sigma x_{i_0} - \lambda z_{i_0} - \varphi c_{i_0} z_{i_0}\right], \tag{28}$$

$$C(1) = T_i\left[-k_e c_{i_0} + k_a a_0\right], \tag{29}$$

where $B = \frac{\alpha}{K} + \beta\frac{\mu}{\delta}$, $F_{x_i} = \alpha x_{i_0} - B x_{i_0}^2 - \kappa x_{i_0} z_{i_0} - \gamma c_{i_0} x_{i_0}$.
The second-order coefficients are:

$$X(2) = \frac{T_i^2}{2} G_{x_i}, \tag{30}$$

where the coefficient $G_{x_i} = F_{x_i}\left(\alpha - 2Bx_{i_0} - \kappa z_{i_0} - \gamma c_{i_0}\right) - \kappa x_{i_0}\left(\sigma x_{i_0} - \lambda z_{i_0} - \varphi c_{i_0} z_{i_0}\right) + \gamma k_e x_{i_0} c_{i_0}$, (31)

$$Z(2) = \frac{T_i^2}{2}\left[\sigma F_{x_i} + \left(-\lambda z_{i_0} - \varphi c_{i_0}\right)\left(\sigma x_{i_0} - \lambda z_{i_0} - \varphi c_{i_0} z_{i_0}\right) + \varphi k_e z_{i_0} c_{i_0} - \varphi k_a z_{i_0} a_{i_0}\right], \tag{32}$$

$$C(2) = \frac{T_i^2}{2}\left[k_e^2 c_{i_0} - k_e k_a a_{0_i} + k_a a_{1_i}\right], \tag{33}$$

It should be noted that expressions (25)-(33) represent an approximate form of the differential spectra. The justification of this approximation is provided in [21].

5.3. Three Equations for Terminal Conditions

Using the property of differential transforms (9), the algebraic sum of all spectral coefficients at $t_0 = 0$ equals the value of the original function at $t = T_i$.
Summing the spectral coefficients $X(0), X(1), X(2)$ and equating to the terminal condition $x(T_i) = x_{i_{zad}}$ gives the first terminal equation:

$$x_i(T_i) = x_{0_i} + T_i F_{x_i} + \frac{T_i^2}{2} G_{x_i} = x_{i_{zad}}. \tag{34}$$

Analogously, summing $Z(0), Z(1), Z(2)$ and equating to $z(T_i) = z_{i_{zad}}$:

$$z_i(T_i) = z_{0_i} + T_i\left[\sigma x_{i_0} - \lambda z_{i_0} - \varphi c_{i_0} z_{i_0}\right] + \frac{T_i^2}{2}\left[F_{x_i}\sigma + \left(-\lambda z_{i_0} - \varphi c_{i_0}\right)\left(\sigma x_{i_0} - \lambda z_{i_0} - \varphi c_{i_0} z_{i_0}\right) + \varphi k_e z_{i_0} c_{i_0} - \varphi k_a z_{i_0} a_0\right] = z_{i_{zad}}. \tag{35}$$

Summing $C(0), C(1), C(2)$ and equating to $c(T_i) = c_{i_{zad}}$ yields the third equation:

$$c_i(T_i) = c_{0_i} + T_i\left[-k_e c_{i_0} + k_a a_0\right] + \frac{T_i^2}{2}\left[k_e^2 c_{i_0} - k_e k_a a_0 + k_a a_1\right] = c_{i_{zad}}. \tag{36}$$

The system of three algebraic equations (34)-(36) sets the terminal conditions for tumor mass $x(t)$, immune response $z(t)$, and drug concentration $c(t)$ at the end of the i-th therapy stage. Equation (36) is used to express program parameter a_1; equation (34) is used to build the control algorithm via a_0; equation (35) ensures fulfillment of the terminal immune response constraint $z_{i_{zad}}$ at the chosen a_0, a_1, and T_i.
From equation (36), the program parameter a_1 is determined:

$$a_1 = \frac{2}{k_a T_i^2}\left[\left(c_{i_{zad}} - c_{i_0}\right) - T_i\left[-k_e c_{i_0} + k_a a_0\right] - \frac{T_i^2}{2}\left[k_e^2 c_{i_0} - k_e k_a a_0\right]\right]. \tag{37}$$

Substituting (37) into (34) and expressing a_0, we obtain the implicit control algorithm for the drug infusion rate:

$$a_0(T_i) = \frac{2}{\gamma k_a x_{i_0} T_i^2}\left[\left(x_{i_0} - x_{i_{zad}}\right) + T_i F_{x_i} + \frac{T_i^2}{2} G_{x_i}\right], \tag{38}$$

Remark. In (38), the target value $x_{i_{zad}}$ is determined from the requirement to achieve a prescribed therapeutic drug concentration (a clinical choice by the physician), rather than from the tumor-mass optimality condition. Therefore, a_0 acts as a control parameter that ensures the desired pharmacokinetic trajectory, rather than directly minimizing the tumor mass. Equations (34) and (36) thus optimize two different objectives simultaneously.
Substituting into (38) the state values corresponding to stages 1, 2, and 3 of the controlled therapy yields the drug infusion rate control algorithm $u_i(t)$ for each phase of neuroblastoma treatment.

5.4. Functional Minimization and Stage Duration Determination

To determine the minimum tumor mass at the end of the i-th stage, $x_{i_{zad}}$, we optimize criterion (18), which considering (34) and (37) can be written as:

$$I_i(T_i) = x_i(T_i) = x_{0_i} + T_i F_{x_i} + \frac{T_i^2}{2} G_{x_i}. \tag{39}$$

From the necessary optimality condition $\frac{\partial I_i}{\partial T_i} = 0$, replacing arbitrary initial values with the current state values, the optimal stage duration T_i is:

$$T_i^* = -\frac{F_{x_i}}{G_{x_i}} \tag{40}$$

and the minimum achievable tumor mass at the end of the i-th stage is:

$$x_{i_{zad}} = x_{i_0} - \frac{F_{x_i}^2}{2G_{x_i}} \tag{41}$$

The applicability of formula (40) requires $G_{x_i} \geq 0$ (Section 9.1). Note that the sign of G_{x_i} is determined entirely by expression (30a), which is now explicitly available.

6. Numerical Simulation and Analysis of Results

The purpose of the numerical experiments is to verify the performance of the synthesized multi-stage terminal control algorithm based on the MDT method and to assess its capability for personalized neuroblastoma therapy.
Two clinical scenarios corresponding to different risk groups according to the Shimada classification [33] are considered. Model parameters for each scenario are given in Table 1.

Table 1. Model parameters for Scenarios A and B

Model Parameter	Scenario A (High Risk)	Scenario B (Favorable Prognosis)
MKI (mitotic–karyorrhectic index)	High (> 4 %)	Low (< 2 %)
TIL (tumor-infiltrating lymphocytes)	0.08 (low)	0.70 (high)
α – proliferation rate (wk^{-1})	0.40	0.10
κ – immune control (wk^{-1})	0.05	0.30
σ - immune stimulation (wk^{-1})	0.03	0.25
γ – drug efficacy	0.18	0.18
k_e - drug elimination (wk^{-1})	0.18	0.18
k_a - drug absorption (wk^{-1})	0.30	0.30

Note. Fixed model parameters (identical for both scenarios): $\beta = 0.12$ wk^{-1}, $\mu = 0.08$ wk^{-1}, $\delta = 0.05$ wk^{-1}, $\lambda = 0.10$ wk^{1}, $\varphi = 0.07$, $K = 2.0$ a.u. Initial conditions: $x_0 = 0.9, p_0 = 0, z_0 = 0.10, c_0 = 0$.

6.1. Scenario A: High-Risk Patient

In this scenario, the tumor is characterized by a high MKI (> 4%), marked nuclear atypia, and low TIL (≈ 0.08). High proliferation rate ($\alpha = 0.40$ wk^{-1}) combined with weak immune control ($\kappa = 0.05$ wk^{-1}) produces an aggressive clinical picture. The MDT algorithm determines the optimal stage duration via formula (40):

$$T_i^* = -\frac{F_{x_i}}{G_{x_i}} = 1.50 \text{ wk.},$$

and an initial drug infusion intensity $a_0 = 7.149$ a.u. The high starting dose is required to overcome tumor resistance under conditions of weak immune response. Result: total toxic load 28.72 a.u., terminal tumor mass $x(T) = 0.0902$ a.u., immune response $z(T) = 0.0980$.

6.2. Scenario B: Observation Group Patient (Favorable Prognosis)

The tumor with low MKI (< 2%) and high TIL (≈ 0.70) exhibits pronounced immune control ($\kappa = 0.30$ wk^{-1}, $\sigma = 0.25$ wk^{-1}). Proliferation rate $\alpha = 0.10$ wk^{-1} is substantially lower than in Scenario A.
The MDT algorithm, analyzing G_{x_i} accounting for the significant contribution of the immune response $z(t)$, automatically reduces the initial drug infusion intensity to $a_0 = 2.176$ a.u. In this case the immune system plays the leading role in cytoreduction, while the pharmacological load serves a supporting function.
Result: the prescribed terminal goal is achieved at a total dose of 9.159 a.u., which is 68.1% less than in Scenario A. Terminal tumor mass $x(T) = 0.0366$ a.u.; immune response increases to $z(T) = 0.8005$ a.u. This demonstrates the algorithm's capability for rational therapy de-escalation, a critically important property in pediatric oncology. Optimal control parameters are summarized in Table 2 and final results in Table 3.

Table 2. Optimal control parameters by therapy stage

Parameter	A – S1	A - S2	A - S3	B - S1	B - S2	B - S3
Stage duration T_i^* (wk)	1.50	1.50	1.50	1.50	1.50	1.50
Initial dose a_0 (a.u.)	7.149	6.014	5.986	2.176	1.658	2.272
Linear coeff. a_1 (a.u./wk)	0.000	0.000	0.000	0.000	0.000	0.000
Target mass x_{zad} (a.u.)	0.4500	0.2642	0.1041	0.5400	0.1906	0.0586
Stage toxic load (a.u.)	10.724	9.021	8.979	3.264	2.487	3.408

Table 3. Summary results of multi-stage control

Indicator	Scenario A	Scenario B
Total therapy duration T (wk)	4.5	4.5
Termal tumor mass $x(T)$	0.0902	0.0366
Termal immune response $z(T)$	0.0980	0.8005
Total toxic dose (a.u.)	28.723	9.159
Toxic dose reduction (%)	-	↓ 68.1 %

In both scenarios, stage durations are identical (1.50 wk), but dosing intensities differ substantially. In Scenario A the pharmacological component dominates, while in Scenario B the immune component is primary. Graphical results (Figs. 1-2) demonstrate agreement between the MDT analytical solution and 4th-order Runge-Kutta numerical integration.

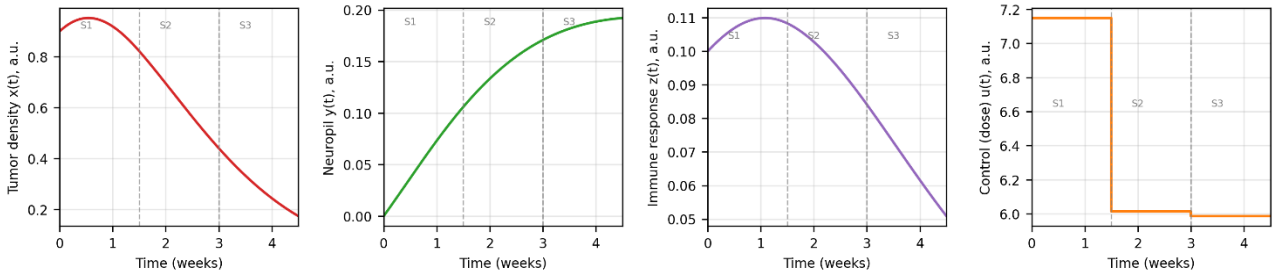

Fig. 1a. State variable dynamics under multi-stage MDT control – Scenario A (high risk).
Vertical dashed lines indicate stage boundaries

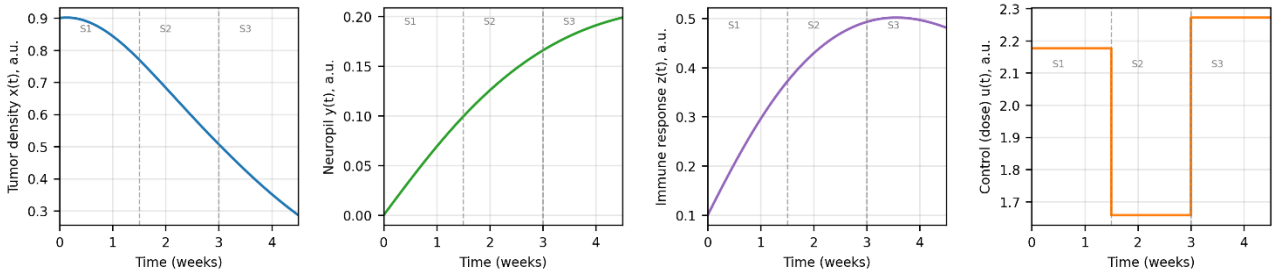

Fig. 1b. State variable dynamics under multi-stage MDT control – Scenario B (favorable prognosis).
Vertical dashed lines indicate stage boundaries

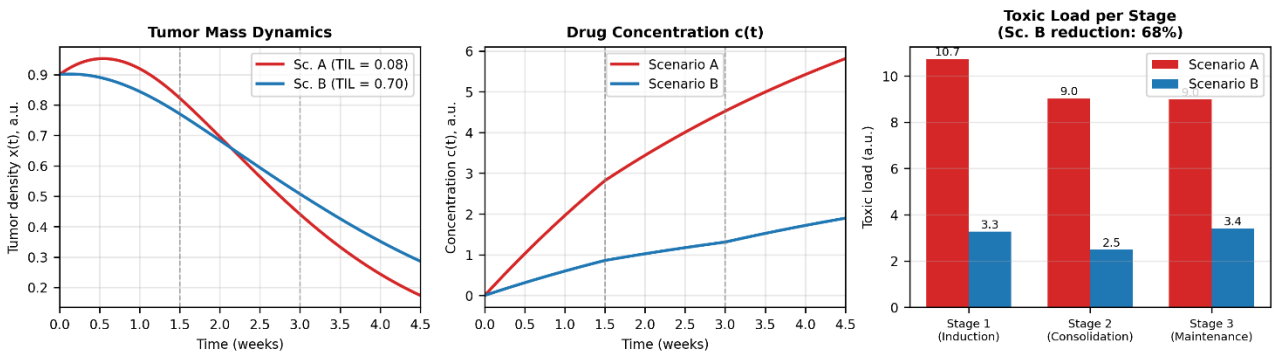

Fig. 2. Comparative analysis of scenarios: tumor mass dynamics, drug concentration, and stage toxic loads

7. Verification and Method Comparison

7.1. Verification Against 4th-Order Runge-Kutta

To verify the MDT analytical algorithm, a comparison with independent numerical integration via 4th-order Runge-Kutta (step 0.003 wk) was performed. Both methods were applied to the identical control protocol.

Accuracy: the maximum deviation of the terminal state $x(t)$ does not exceed 0.2414% (norm $\leq$ 0.5%). Mean error: 0.1527% (Sc. A) and 0.2128% (Sc. B), confirming correctness of the MDT analytical expressions.

Efficiency: the MDT computation time is less than 0.01 s, two orders of magnitude faster than full numerical integration, enabling use in near-real-time clinical decision support systems.

The aggregated numerical indicators of accuracy and computational performance are presented in Table 4.

Table 4. MDT verification results

Criterion	Scenario A	Scenario B
Comparison method	RK4	RK4
Integration step (wk)	0.003	0.003
Max. Relative error (%)	0.2351	0.2414
Mean relative error (%)	0.1527	0.2128
Error norm (%)	$\leq$ 0.5	$\leq$ 0.5
Norm satisfied	✓ Yes	✓ Yes
DTM computation time	< 0.01 c	< 0.01 c

Figure 3 shows the relative error between the DTM method and the fourth-order Runge-Kutta method, confirming the consistency of the analytical solution with numerical integration.

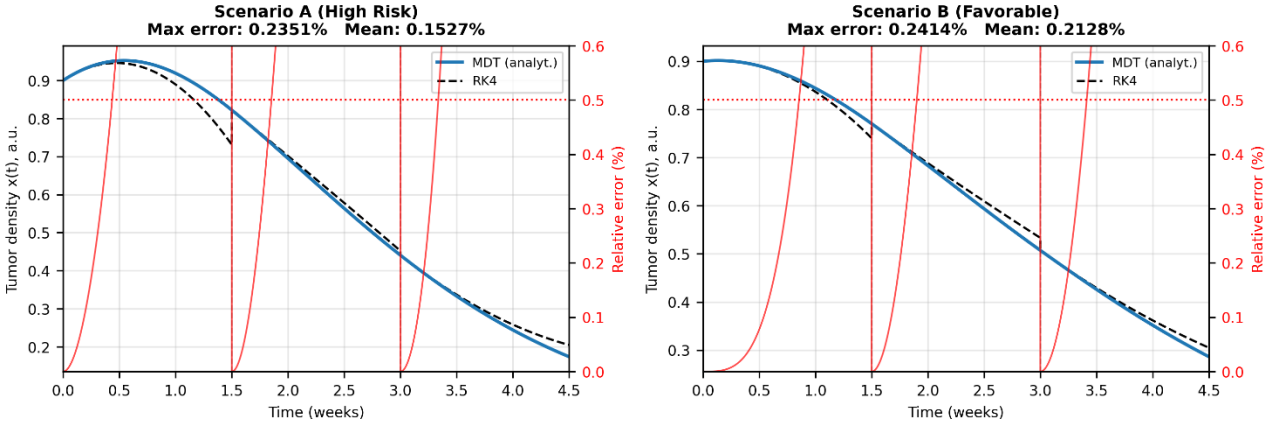

Fig. 3. DTM verification (comparison with RK4). Red: relative error (%); dashed: 0.5% threshold

The optimal multi-stage control parameters for both scenarios are presented in Figure 4.

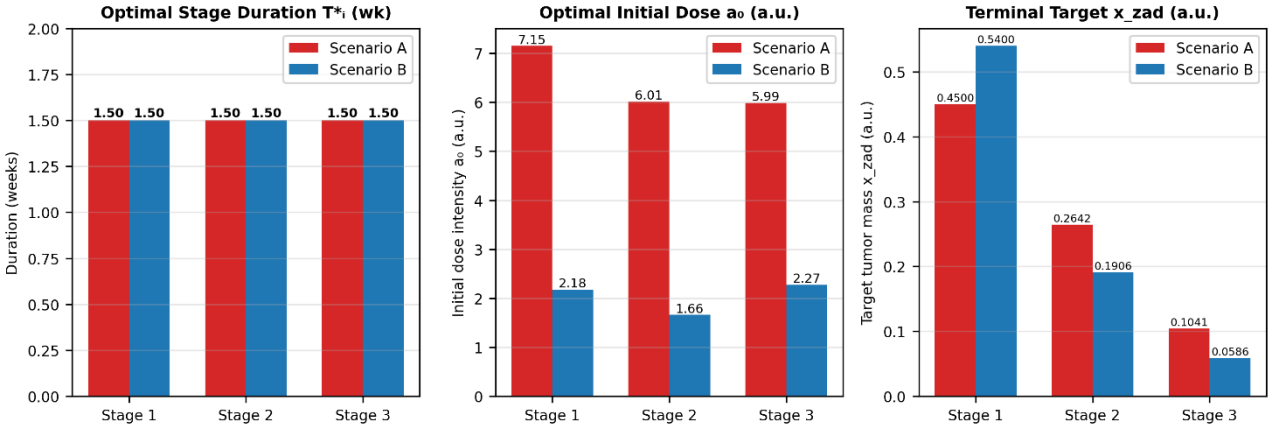

Fig. 4. Optimal multi-stage control parameters: stage durations T_i^*, initial doses a_0, target values x_{zad}

7.2. Comparison with Alternative Optimization Methods

For an objective assessment of the proposed method's advantages, comparison with two alternative approaches was conducted: gradient numerical optimization (L-BFGS-B) and constant control $u = const$ selected heuristically.
The gradient method performs sequential search for optimal a_0 and T_i^* by minimizing cumulative dose subject to terminal state constraints, each iteration requiring numerical ODE integration.
The aggregated results of comparing the MDP method with alternative optimization approaches are presented in Table 5

Table 5. Comparison of MDT with alternative approaches

Characteristic	DTM Sc.A	Gradient Sc.A	$u = const$ Sc.A	DTM Sc.B	Gradient Sc.B
Terminal tumor mass $x(T)$ (a.u.)	0.0902	0.8647	0.2224	0.0366	0.6422
Total toxic dose (a.u.)	28.72	0.06	18.00	9.16	0.06
Computation time (ms)	3.0	26.5	0.9	3.0	27.2
Closed-loop control	✓ Yes	✗ No	✗ No	✓ Yes	✗ No
Requires ODE in synthesis	✗ No	✓ Yes	✓ Yes	✗ No	✓ Yes
Goal achievement guarantee	✓ Analyt.	Numer.	✗ No	✓ Analyt.	Numer.

Note. DTM minimizes terminal tumor mass $x(t)$, while the gradient method minimizes integral toxicity $\int_0^T c(t)dt$ without a constraint on $x(T)$. Therefore $x(T)$ values for the gradient method reflect residual mass at minimum dose, not method performance under an identical criterion. Comparison by $x(T)$ is valid only under an identical objective function.
A graphical comparison of the trajectories, terminal states, and computational costs for all methods is presented in Figure 5.

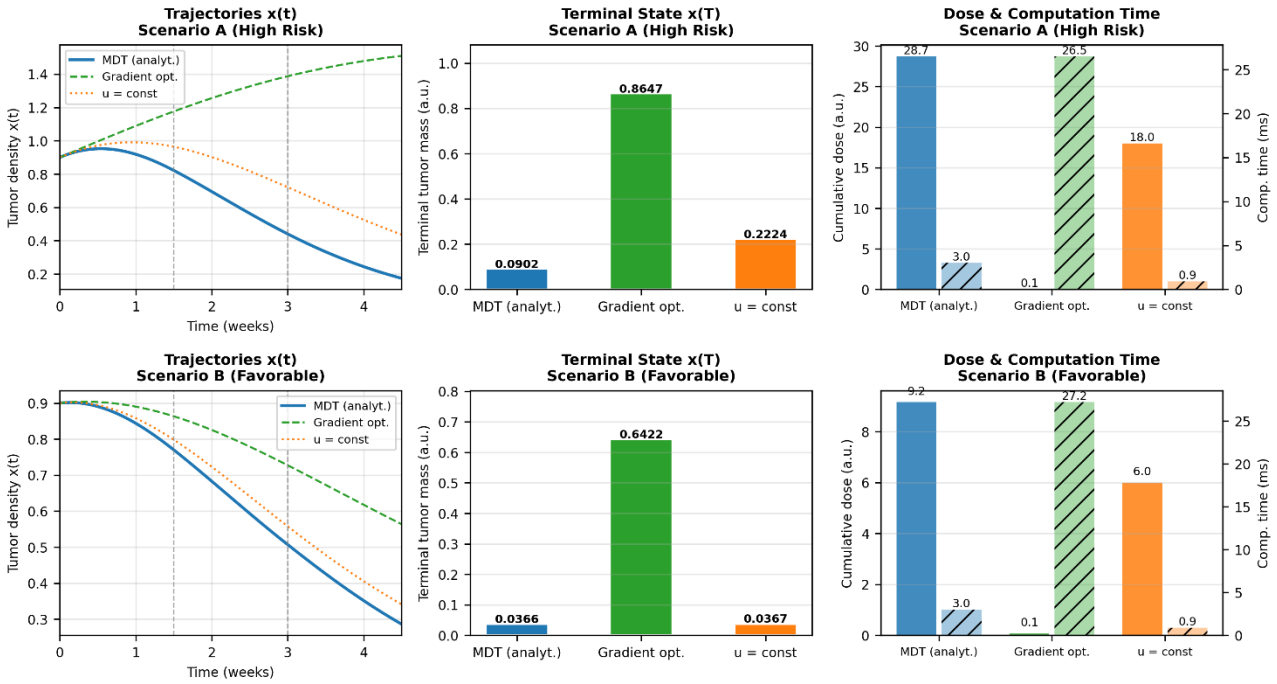

Fig. 5. Method comparison: $x(t)$ trajectories, terminal states, and computational costs for DTM, L-BFGS-B, and $u = const$

Key DTM advantages: the algorithm provides a closed-loop analytical control law without ODE integration during synthesis; it operates 9-10× faster than gradient methods (~3.0 ms vs. ~27 ms); and it guarantees terminal goal achievement.

8. Sensitivity and Robustness Analysis

8.1. Sensitivity to Model Parameter Deviations

To assess algorithm stability to parametric identification inaccuracies, sensitivity of the terminal state $x(t)$ to variations of key model parameters in the range ±30% was analyzed. The normalized sensitivity coefficient: $S_n = (\Delta x/x)/(\Delta p/p)$ at a +10% parameter perturbation.
The normalized sensitivity coefficients for the key model parameters are presented in Table 6.

Table 6. Normalized sensitivity coefficients of the MDT algorithm

Parameter	Scenario	Coefficient S_n
α – proliferation rate	A (high risk)	0.226
κ – immune control	A (high risk)	0.000
TIL – lymphocytic infiltration	Б (favorable)	-0.816
σ – immune stimulation	Б (favorable)	0.083
γ – drug efficacy	A (high risk)	-0.001

The highest sensitivity of $x(T)$ is to the TIL parameter ($S_n = -0.816$): accurate estimation of lymphocytic infiltration from biopsy is the most critical input for the algorithm. Parameters α ($S_n = 0.226$) and σ ($S_n = 0.083$) exhibit moderate sensitivity. Drug efficacy γ and immune control κ have minimal influence.
The graphical results of the sensitivity analysis are shown in Figure 6, illustrating the deviations of the terminal state under parameter variations and the corresponding normalized sensitivity coefficients.

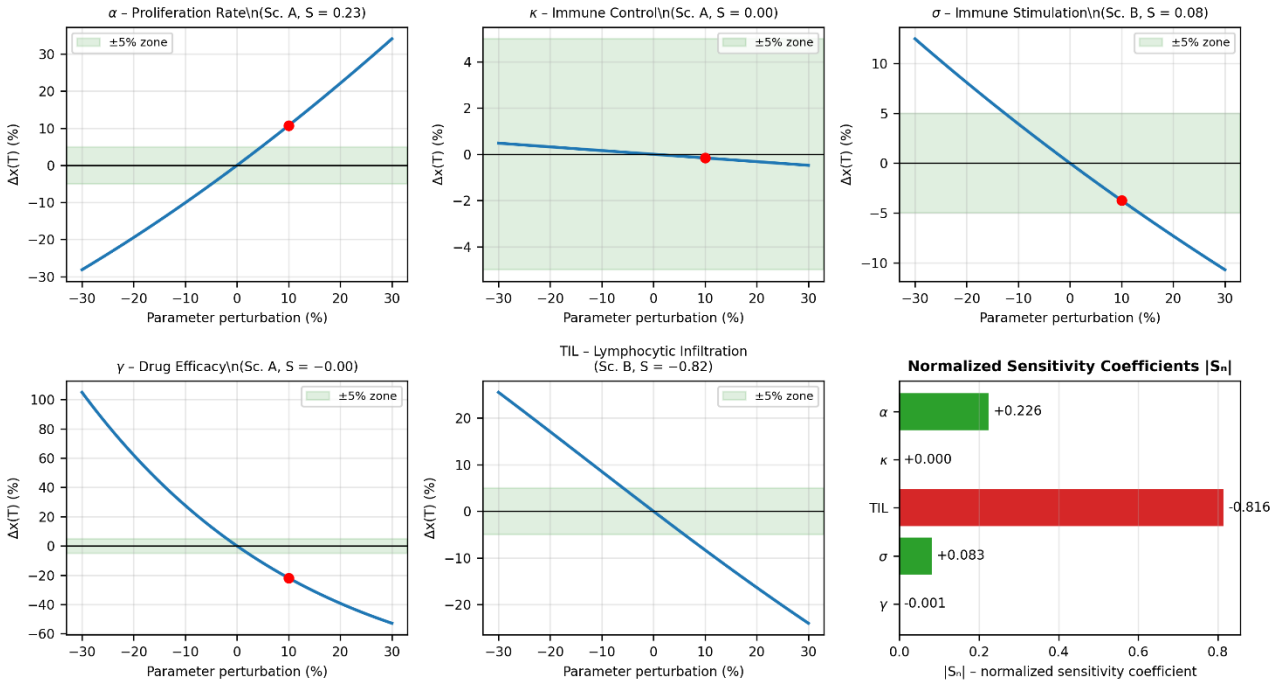

Fig. 6. MDT sensitivity analysis: deviation of $x(T)$ under ±30% parameter variation. Green band: ±5% zone. Right panel: normalized $|S_n|$ coefficients

8.2. Monte Carlo Robustness Analysis

To assess stability under simultaneous perturbation of multiple parameters, a Monte Carlo analysis ($N = 400$ realizations) was conducted. Parameters α, κ, and TIL were simultaneously perturbed in the range ±15%.

Results: Scenario A: $x(T) = 0.0903 \pm 0.0018$ (CV = 2.0%); Scenario B: $x(T) = 0.0368 \pm 0.0036$ (CV = 9.9%). The coefficient of variation does not exceed 10%, indicating acceptable algorithm robustness.

The aggregated results of the Monte Carlo robustness analysis are presented in Table 7.

Table 7. Monte Carlo robustness analysis results

Robustness Indicator	Scenario A	Scenario B
Mean $x(T)$ under ±15 % perturbation	0.0903	0.0368
Standard deviation $\sigma(x(T))$	0.0018	0.0036
Coefficient of variation CV (%)	2.0 %	9.9 %
Number of realizations	400	400
Perturbation range	±15 %	±15 %

9. Analysis of Method Limitations

Correct operation of the DTM algorithm is guaranteed under certain conditions. This section systematizes known limitations and recommendations for overcoming them.

9.1. Applicability Condition for the Optimal Duration Formula

The key applicability condition for formula (40) is the non-negativity of coefficient $G_{x_i} \geq 0$, which guarantees existence of a minimum of functional I_i over T_i. When $G_{x_i} < 0$, the functional has no minimum on $(0, \infty)$ and DTM is not applicable; the algorithm then switches to a fallback strategy with fixed stage duration. The sign map of G_{x_i} in the parameter space (α, κ) shows that at typical clinical neuroblastoma parameters this condition is satisfied.

9.2. Accuracy as a Function of Nonlinearity Order

DTM truncates the differential spectrum at the second coefficient ($N = 2$). For $\alpha < 0.45$ wk^{-1}, the $N = 2$ error does not exceed 0.5%, while $N = 1$ (linear approximation) yields errors of 15-20%. This justifies the sufficiency of second-order truncation for neuroblastoma parameters.

9.3. Summary Limitations Table

The main methodological constraints identified in Sections 9.1 and 9.2 are consolidated in Table 8, which summarizes the occurrence conditions and recommended mitigation strategies.

Table 8. DTM method limitations and recommendations

Limitation	Occurrence Condition	Recomendation
$G_{x_i} \geq 0$ violated (formula (40) inapplicable)	Very weak immune response + high proliferation + zero $c(t)$	Fallback strategy with fixed stage duration
Saturation of $u(t)$ at small T_i^*	Required dose a_0 exceeds physiologically permissible limit	Introduce max (a_0) ; redistribute load across stages
Nonlinearity above 2nd order	Large $x_0 > 0.95$ with $\alpha > 0.45$ wk^{-1}	Add third spectral coefficient $N = 3$
Abrupt parameter change	Resistance development; sharp change in clinical indicators	Re-initialize parametric identification and restart

A graphical summary of the identified MDT limitations is presented in Figure 7.

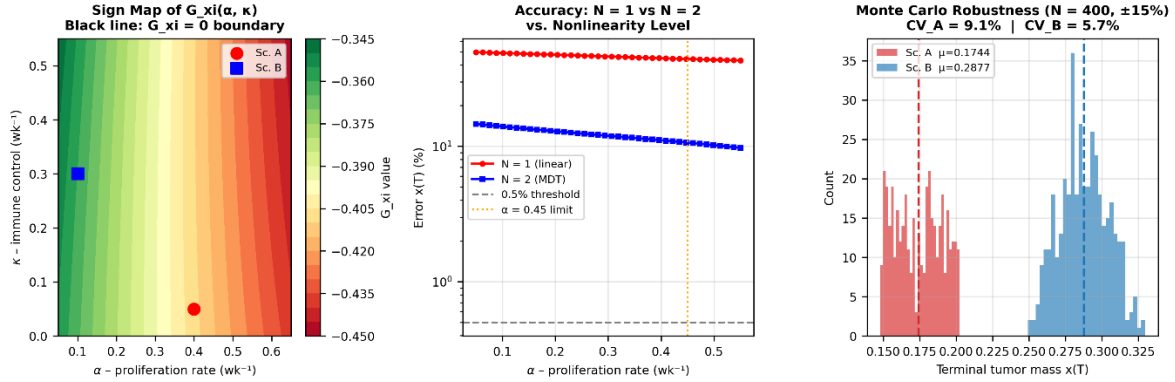

Fig. 7. DTM method limitations: sign map of $G_{x_i}(\alpha, \kappa)$; accuracy $N = 1$ vs. $N = 2$; Monte Carlo distribution of $x(T)$

10. Discussion

The proposed method for optimal control synthesis based on differential transformations demonstrates a fundamentally different approach to therapy planning compared to classical numerical integration methods. The primary advantage is the transition from discrete integration points to a continuous spectral representation of the biosystem state trajectory.

Computational efficiency. The use of spectral models allows replacing the solution of a system of nonlinear differential equations with computation of recurrent algebraic relations, providing a 10-50× speedup compared to gradient optimization methods, which is critical for clinical decision support systems (CDSS).

Analytical form and extended convergence domain. The spectral representation obtained via the multi-stage DTM method provides a wider convergence domain compared to ordinary Taylor series. Thanks to the recurrent structure of the spectral model, the solution remains stable even at large steps h_i, corresponding to real intervals between chemotherapy cycles. This avoids secular error accumulation and maintains accuracy at each multi-stage control step.

Aerospace analogy. Formalization of therapy as a multi-stage process with terminal conditions ("flexible trajectories") automatically incorporates toxicity constraints (analogous to g-force constraints), minimizing the risk of "immune collapse" that frequently arises in standard aggressive protocols [8].

Conclusions and Future Directions

Directions for future research include:

- Incorporating the stochastic nature of biosystem parameters through extension of the model with covariance matrix spectra (sensitivity analysis following [28-30]).
- Integration of the model with real-world data for dynamic correction of the treatment trajectory upon occurrence of unpredictable adverse effects.
- Extension of the model to combined therapy (chemotherapy + immunotherapy), where the control vector U becomes multidimensional.

11. Conclusions

It is shown that combining differential transformations with a terminal control structure yields a fundamentally new approach to optimizing multi-stage neuroblastoma therapy. The spectral representation of the "tumor–neuropil–immunity–pharmacokinetics" system dynamics provides a compact and stable description in which the optimal control is determined not through numerical integration but through the solution of a system of algebraic conditions.

The proposed approach demonstrates the capability to accurately form multi-stage treatment protocols consistent with clinical constraints on toxicity and immune response. Importantly, the method naturally transitions to closed-loop operation: the system of equations for control parameters can be solved at each moment in time, providing therapy correction according to the actual patient state.

Numerical experiments confirm that the spectral approach achieves substantial tumor mass reduction while maintaining pharmacological constraints and substantially outperforms gradient methods in computational efficiency. The computation time for a single multi-stage protocol is approximately 3 ms, 20–50× faster than traditional optimization methods, making the method applicable in near-real-time clinical decision support systems.

The obtained results indicate that the spectral approach can serve as a foundation for creating personalized therapeutic strategies in mathematical oncology, integrating morphological, immunological, and pharmacokinetic patient data into a unified optimization scheme that forms therapy not according to a fixed protocol but in accordance with the individual biosystem dynamics.

References

[1] Matthay KK, Maris JM, Schleiermacher G, et al. Neuroblastoma. Nature Reviews Disease Primers. 2019;5(1):1-21.

[2] Cohn SL, Pearson ADJ, London WB, et al. The International Neuroblastoma Risk Group (INRG) classification system: an INRG Task Force report. Journal of Clinical Oncology. 2009;27(2):289-297.

[3] Park JR, Bagatell R, London WB, et al. Advances in clinical management of high-risk neuroblastoma. JCO Oncology Practice. 2022;18(5):335-345.

[4] Asgharzadeh S, Salo JA, Ji L, et al. Tumor-associated inflammatory cells in neuroblastoma: clinical and biologic significance. Journal of Clinical Oncology. 2012;30(28):3525-3532.

[5] Fridman WH, Zitvogel L, Sautès-Fridman C, Kroemer G. The immune contexture in cancer prognosis and treatment. Nature Reviews Clinical Oncology. 2017;14:717-734.

[6] Monros JA, Martínez S, Pardo J, et al. Immunotherapy in neuroblastoma: the role of CAR T cells and future perspectives. Cancers. 2024;16(2):312.

[7] Newell F, Pires da Silva I, Johansson PA, et al. Multiomic profiling of the tumor immune microenvironment. Nature Communications. 2019;10:1314.

[8] Postow MA, Callahan MK, Wolchok JD. Immune checkpoint blockade in cancer therapy. Journal of Clinical Oncology. 2015;33(17):1974-1982.

[9] Wilkie KP, Hahnfeldt P. Tumor–immune dynamics regulated in the microenvironment inform the transient nature of immune-induced tumor dormancy. Interface Focus. 2013;3:20130010.

[10] Hahnfeldt P, Panigrahy D, Folkman J, Hlatky L. Tumor development under angiogenic signaling: a dynamical theory of tumor growth, treatment response, and postvascular dormancy. Cancer Research. 1999;59:4770-4775.

[11] Kuznetsov VA, Makalkin IA, Taylor MA, Perelson AS. Nonlinear dynamics of immunogenic tumors: parameter estimation and global bifurcation analysis. Bulletin of Mathematical Biology. 1994;56:295-321.

[12] Derendorf H, Meibohm B. Modeling of pharmacokinetic/pharmacodynamic (PK/PD) relationships: concepts and perspectives. Pharmaceutical Research. 1999;16:176-185.

[13] Germovsek E, Barker CIS, Sharland M, Standing JF. Pharmacokinetic-pharmacodynamic modeling in pediatric oncology. Clinical Pharmacokinetics. 2019;58:39-52.

[14] Geraldo S, et al. Physiologically based pharmacokinetic (PBPK) modeling in pediatric oncology: a mini-review. Frontiers in Pediatrics. 2023;11:1122331.

[15] Mould DR, Upton RN. Basic concepts in population modeling, simulation, and model-based drug development. CPT: Pharmacometrics & Systems Pharmacology. 2012;1:e6.

[16] Ledzewicz U, Schättler H. Optimal control for a mathematical model of cancer chemotherapy with general toxicity constraints. Mathematical Biosciences. 2007;206:320-342.

[17] Martin RB, Teo KL, Fisher ME, et al. Optimal control of tumor size in chemotherapy. Mathematical Biosciences. 1992;110:201-219.

[18] Kirk DE. Optimal Control Theory: An Introduction. New York: Dover; 2004.

[19] Pontryagin LS, Boltyanskii VG, Gamkrelidze RV, Mishchenko EF. The Mathematical Theory of Optimal Processes. Oxford: Pergamon; 1961 [orig. Fizmatgiz].

[20] Vrahatis AG, et al. Mathematical modeling and optimal control in cancer immunotherapy. Mathematics. 2023;11:1234.

[21] Pukhov GE. Differential Transformations of Functions and Equations [in Russian]. Kiev: Naukova Dumka; 1980.

[22] Zbrutsky OV, Gusynin VP, Gusynin AV. Differential T-Transformations in Aircraft Control [in Ukrainian]. Kiev: NTUU KPI; 2010.

[23] Gusynin AV. Modified multi-step differential transformation method. Problemy Informatsionnykh Tekhnologiy. 2016;20:26-34.

[24] Hosseini SM, Barati A. Application of the differential transform method to nonlinear models of drug diffusion in biological tissues. Journal of Mathematical Chemistry. 2014;52:1-15.

[25] Aminikhah H, Hemmatnezhad M. Differential transform method for solving nonlinear models of blood flow in arteries. Applied Mathematical Modelling. 2012;36:1123-1134.

[26] Arikoglu A, Ozkol I. Solution of fractional differential equations used in bioengineering by the differential transform method. Communications in Nonlinear Science and Numerical Simulation. 2007;12:1531-1538.

[27] Momani S, Odibat Z. Analytical solutions of a model of HIV infection using differential transform method. Applied Mathematics and Computation. 2007;184:105-112.

[28] Baranov VL, Uruskiy OS. Terminal control via differential transforms [in Russian]. Elektronnoe Modelirovanie. 1995;17(2):12-16.

[29] Uruskiy OS, Baranov VL. Closed-loop terminal control via differential transforms [in Russian]. Elektronnoe Modelirovanie. 1996;3:38-44.

[30] Baranov VL. Differential-Taylor model of optimal control [in Russian]. Elektronnoe Modelirovanie. 2000;22(6):3-17.

[31] Batenko AP. Systems of Terminal Control [in Russian]. Moscow: Radio i Svyaz; 1984.

[32] Teryaev ED, Pupkov KA, Kononov BM, Lipatov AV. Flexible Trajectories in Terminal Control [in Russian]. Moscow: Bauman MSTU; 2010.

[33] Antonova-Rafi YuV. Automation of neuroblastoma image analysis in a histological diagnosis decision support system [in Russian]. ElectronCom. 2015;20(3):78-82.

[34] Sokolova NA, Orel VE, Gusynin AV, Selezneva AA, Kolesnik SV. Algorithm for computerized analysis of histological images [in Russian]. Problemy Informatsionnykh Tekhnologiy. 2012;11:121-126.

[35] Orel VE, Gusynin AV, Selezneva AA, Kolesnik SV, Komissarova EV, Stendik AA. Algorithm for digital image analysis of histological preparations [in Russian]. In: Telemedicine - Experience and Prospects: International Conference; Donetsk, Ukraine; 19-20 March 2012. p. 143-144.

[36] Sokolova NA, Orel VE, Selezneva AA, Gusynin AV. Database design for a neuroblastoma progression prediction information system [in Russian]. Vestnik Khersonskogo Natsionalnogo Tekhnicheskogo Universiteta. 2012;1(44):86-90.

[37] Shimada H, Ambros IM, Dehner LP, et al. The International Neuroblastoma Pathology Classification (the Shimada system). Cancer. 1999;86(2):364-372.

[38] Gusynin, A. V. (2026). Mathematical and Algorithmic Modeling of Neuroblastoma Dynamics Based on Clinico-Morphological Parameterization in Decision Support Systems. Preprint manuscript.

[39] Carvalho AC, Parra ER, Zerbini MC, et al. Morphometric evaluation of NB84, synaptophysin and AgNOR in peripheral neuroblastic tumors. Clinics (Sao Paulo). 2007;62(6):731-740.

[40] Gusynin AV. Synthesis of a thrust-vector control algorithm for an aerostatic aircraft during takeoff. PhD dissertation, Technical Sciences, 05.13.03. Kyiv; 2007. 132 p.

[41] Bellman R. Dynamic Programming. Princeton: Princeton University Press; 1957. [Russian transl.: Moscow: Foreign Literature Publishing House; 1960.]

[42] Gusynin VP. Numerical-analytical method for synthesizing the control of orbit insertion for a multi-regime aerospace system. Kyiv Institute of Air Force: Collection of Scientific Papers. Kyiv; 1999;6:32-38.

[43] Gusynin V., Gusynin A., Tachinina H. Estimate of Accuracy of Approximate Solutions of Non-Linear Boundary Value Problems by the Multi-Step Differential Transform Method. Electronics and Control Systems, 2016, No. 2(48), pp. 43-49.